RSC Advances

ROYAL SOCIETY OF CHEMISTRY

www.rsc.org/advances

Plasmonic absorption activated trapping and assembling of colloidal crystals with non-resonant continuous gold films

Zhiwen Kang, Jiajie Chen, Shu-Yuen Wu, and Ho-Pui Ho*

Department of Electronic Engineering, The Chinese University of Hong Kong, Shatin, N.T., Hong Kong SAR, China

*Corresponding email: hpho@ee.cuhk.edu.hk

Abstract: Here we report the realization of trapping and assembly of colloidal crystals on continuous gold thin films based on the combined effect of thermophoresis and thermal convection associated with plasmonic optical heating. In the system, the stabilized trapping phenomenon is driven by thermophoretic forces caused by temperature gradient which push the target particles from cold to hot region and are always in opposite direction to the axial convective drag forces. Furthermore, the lateral convective flow of aqueous medium accelerates the formation of the trap considerably by dragging target particles into the hot region from a long distance. The influence of salt concentration on the trapping behavior has also been investigated. Typically the threshold optical power density is in the order of microwatts per square micrometer (~ $\mu W / \mu m^2$). We anticipate that the reported optical trapping approach may find many potential applications in biophysics, life science, and lab-on-a-chip devices.

Keywords: Continuous gold film; Optical heating; Thermophoresis; Convection; Ion concentration.

Introduction

Optical tweezers offer a noninvasive technique by using light to trap and manipulate small objects. This approach has been developed for several decades and widely applied in physics, biochemistry, and life sciences.[1-3] Its operation relies on the use of tightly focused laser beam that produces a strong intensity gradient force, which attracts small objects along the gradient to the region of maximum intensity due to polarized electric field interactions.[4] With the development of nanotechnology, optical manipulation has become increasingly stringent in terms of incident light density and target position accuracy. These requirements have been partially addressed through the use of localized surface plasmons excited in gold nanostructures. Plasmonic effects result in considerable enhancement in nanoscale optical confinement, therefore leading to very strong gradient force for trapping with low power threshold.[5-7] Plasmonic nanostructures such as cavity,[8] antenna,[9, 10] dimer,[11] square lattice,[12] ring,[13] disks,[14, 15] tapered fibre,[16] etc., have been reported to be capable of performing nano-optical trapping. However, because of inevitable plasmonic absorption, local optical heating always occurs alongside the trapping process.[10-12] In fact, integration of a heat sink for efficient removal of thermal effects (long-range interaction) can improve the effectiveness of the optical trap (short-range interaction).[17] However, as also shown in this work, thermal effects may not be totally regarded as a negative contribution.

First, an increase in local temperature causes the fluid density to decrease, while leads to natural convection flow driven by buoyancy. The flow has a typical toroidal shape with the fluid being pushed into and out of the hot zone radially as well as vertically.[18, 19]

Particles that are far away from the illuminated region will also be dragged into the hot zone by the convective flow. Without the assistance of convention, it may take approximately 4 hours for Brownian motion to drive the particles to the trap.[20] Second, the local temperature gradient induces an inhomogeneity at the particle-solvent interface. This interfacial effect, namely thermophoresis, may cause the particles to move between cold and hot regions depending on the sign of the Soret coefficient.[21, 22] It is reported that the Soret coefficient can be affected by particle size,[23] temperature,[24] solvent pH and surface charge, which can be altered by the addition of salt,[25] and the comprehensive understanding of thermophoresis is still in progress.[26, 27]

Recently, we reported the trapping of particles on large-scale random gold nano-islands.[28] We showed that short-range near-field optical trapping force alone is not strong enough to counteract the long-range axial convective drag force and thermophoretic force plays an important role in the observed trapping phenomenon by pushing the target particles from cold to hot region. As an extension of that work, which offers a strong possibility of more widespread application due to the ease of substrate preparation, we herein report the trapping and assembling of colloidal particles on continuous gold thin films with incident threshold power density as low as several microwatts per square micron. The trapping mechanism relies on thermophoresis, which stabilizes the trap by overcoming the axial upward convective drag force. We have characterized the trapping performance in relation to the increase of temperature with respect to film thickness and the concentration of salt in the solvent (i.e. water). It is found that salt concentration levels of 10^{-4} mol or higher will significantly reduce thermophoretic

force and eventually quench the trapping effect.

Materials and methods

The continuous gold thin film was deposited directly on microscope cover glass (Ted Pella Inc.) using conventional DC sputtering (KYKY Technology Development Ltd.). In this study we prepared four samples with nominal thickness of 10, 30, 50, and 70 nm. The deposition rate was 0.1 nm/s and the base pressure during sputter deposition was 1.0 Pa. Generally, increasing the film thickness would result in reducing the optical transmission coefficient. In our experiments, we visually inspected the samples [right, Fig. 1(a)] and the extinction spectra [left, Fig. 1(a)] was measured with a UV–visible/NIR spectrophotometer (Hitachi U-3501). From atomic force microscope (AFM) [Figs. 1(b)-1(e)], one can see that the surface of the continuous thin film is not completely flat. Instead, the sample surface contains a large number of small grains, gaps, and voids. Indeed this kind of surfaces also have random plasmonic effects, i.e. random regions having highly localized near-field intensity akin to “hot-spots” in surface-enhanced Raman scattering which are associated with rough metal surfaces.[29] As measured from the AFM images, the root mean square (RMS) of roughness are 0.587, 0.602, 0.753, and 0.677 nm, for the 10, 30, 50, and 70 nm thin films, respectively.

The experiments were conducted on a Nikon inverted microscope (TE2000-U) as depicted in Fig. 2. A linearly polarized laser beam (λ=785 nm) from a semiconductor diode was focused on the Au film via an oil-immersion objective [60×, numerical aperture (NA)=1.49], and the diameter of laser spot was 12 μm. Images of the sample were

captured using a charge-coupled device (CCD) camera through the same lens. The laser beam was not expanded to fill the entrance of the objective lens, and hence the laser spot was not focused to the ultimate diffraction-limited spot size achievable by the objective. A band-reject filter was inserted to block the trapping laser beam. The particles we studied were polystyrene spheres (PS) with diameters of 0.5 μm and 1.5 μm (Polysciences Inc.). The PS were suspended in deionized water or salt solution with various concentration levels and the concentration was about 1.1×10^9 particles/mL. During a typical trapping experiment, a 20 μL droplet of the suspension was placed directly on the sample surface. The laser power on the sample surface was adjustable between four levels, with P1 to P4: 1.0, 3.7, 9.2, and 14.5 mW, corresponding to power densities of 8.8, 32.7, 81.3, and 128.2 $\mu W/\mu m^2$, respectively.

Results and Discussion

Our experiments reveal that samples with different thicknesses exhibit various degrees of trapping behaviour. Representative images are shown in Figs. 3(a) and 3(b) for the 30 nm and 50 nm thin films, both at P3 (9.2 mW), respectively. During the experiment we noticed that trapping of PS particles towards the illuminated region occurred immediately after bringing in the laser beam. First, the long range (larger than 30 μm) lateral convective flow induced by plasmonic absorption brought the particles towards the hot centre (see Fig. 2), then thermophoresis force in a direction opposing to the axial convection stopped the particles from being pushed away, the trapped particles automatically arranged themselves to form a tightly packed hexagonal assembly. When

we switched off the laser, the assembly dispersed under Brownian motion. The assembling of colloidal particles on continuous gold thin films has been widely investigated,[30-34] however, these self-assembly techniques require a long time for the particles to settle and the solvent to dry. On the other hand, our approach offers the flexibility to form self-assembling at any location as desired, and the process takes very short time.

Given the fact that our continuous gold film contains a large number of small random gaps in the surface, pure optical trapping due to field localization and enhancement of gradient field should be present. However, the gradient field only occurs within a distance of 20 nm from the surface.[13, 28, 35] Clearly this is not sufficient to overcome the long-range force due to upward axial convective flow (see Fig. 2). Yet our experiments have revealed the existence of a stable trap. We attribute the observed trapping phenomenon to an additional force component associated with the thermophoretic effect, which has a magnitude larger than that of the axial convective drag force and pushes the PS targets from cold to hot region (see Fig. 2). Moreover, once the trap is established, one can readily move the trapped PS to any location on the sample surface as they follow the movement of focused laser spot. Trapping and assembling of live bacteria (*Escherichia coli*) on such continuous thin films can also be achieved. It should be noted that, because of the large area of laser spot (diameter of 12 μm), the laser power density within the trapping region is only 81.3 $\mu W / \mu m^2$, even though a laser power of 9.2 mW (P3) has been used in the present case.

We have performed a series of experiments to study the statistical characteristics of

the observed trapping phenomenon. The population of PS within the trapping mode as a function of time for the samples that have nominal thickness of 10 to 70 nm are summarized in Fig. 4 (a)-(d), respectively. Indeed our experiments confirm that the number of PS within the assembly increases exponentially with time. This is a direct consequence from the fact that the trapping potential well has a Gaussian profile. When the PS are being drawn towards the trapping zone, they begin to fill up the potential well from the bottom until it is fully occupied. Since the potential is directly related to the population statistics of the particles via the Boltzmann distribution,[36] an increase in the number of PS trapped in the zone also means that the potential well depth will increase as the well volume tries to accommodate more particles. For the 10 nm thin film, laser power at P1 and P2 corresponds to an average trapping capacity of 28 and 72 PS. Also, for this sample a laser power level of P3 or P4 will not produce a stable trap due to the presence of strong thermal convection as the high laser power has induced severe local heat of the solvent round the hot zone. For the 30 nm thick thin film, laser power levels at P1 through to P4 can provide mean trap capacities of 22, 122, 198, and 218 PS respectively. For the 50 nm case, the capacity increases from 26 to 308 upon increasing the laser power from P1 to P4, while for 70 nm, the capacity increase is from 56 to 430. Further increase in film thickness has led to lower light transmission, which results in a reduction in trapping strength. For example, laser power at P4 only gives rise to trapping of 390, 205, and 135 PS for nominal film thicknesses of 90, 110, and 130 nm respectively. In Fig. 4 (e), we show trapping of PS with 0.5 μm and 1.5 μm on 10 nm gold film using laser power P2 (3.7 mW) and spot size of 12 μm. Given that the power density, and hence the trap

potential is the same for both cases, the total trapping volume should also be the same. We consequently see that fewer 1.5 μm PS have been trapped as compared to the 0.5 μm ones because of their larger size. These trapping results are consistent with the analysis reported in Ref.28.

If one uses a large NA (=1.49) objective, surface plasmon polaritons (SPPs) excitation can be possible in continuous thin films. [37] Indeed, this is due to scattering from small grains/spikes in the Au film, which have been revealed by AFM to be present in the samples. The circular SPP wavefront as excited from the converging incident laser beam will propagate towards the centre of focal spot. This may lead to a lateral force that pushes the target particles to the centre of the trap. However, our experiments suggest that the contribution of SPPs towards trapping is negligible because a small NA (=0.6) objective has been used. At this value of NA, the angle of incidence is not shallow enough to produce efficient excitation of SPPs (see Fig. 5). This further confirms that the observed trapping phenomenon is solely associated with thermal effects.

The time-averaged arrival velocities of PS within the trapping process were measured by monitoring their motion through analysing recorded image sequences frame by frame. The drag force exerted on the PS is calculated by applying the Stokes law $F = \mu v$, where $\mu = 3\pi\eta D$ is the drag coefficient with η the dynamic viscosity and D the diameter of PS, and v is the velocity of particle.[5, 10] The temperature dependence of η is considered in the calculation.[38] As shown in Fig. 6, upon increasing the laser power the velocity (drag force) also increases from 5.10 to 8.85 μm/s (23 to 40 fN), from 4.65 to 13.60 μm/s (21 to 59 fN), from 5.06 to 12.84 μm/s (23 to 57 fN), and from 4.52 to

13.55 μm/s (21 to 60 fN), for the 10, 30, 50, and 70 nm cases respectively. The particle motion is essentially driven by the long-range interactions originated from thermal convection. The direction of the measured drag forces is lateral, i.e. parallel to the film surface. Vertical convection has the same velocity as that of the lateral direction (see Fig. 2), i.e. vertical upward drag force has the same magnitude as the lateral force.[18, 19, 28, 29, 39] Therefore, the downward force originated from the thermophoresis should be larger than that vertical drag force in order to have a stable assembly of trapped PS.

In addition, we have indirectly measured the local temperatures of all sample surfaces in order to gain a better understanding of the thermal effects. Our experiment was based on measuring the fluorescence efficiency of Rhodamine B (0.1 mM solution) whose temperature dependence has been well documented.[28, 40, 41] In the experiment, the room temperature was 21 ^{o}C, and after pre-calibration and data fitting, we carried out the temperature measurement on all the thin film surfaces when illuminated by the 785 nm laser beam. As the laser power increased stepwise from P1 to P4, the surface temperature of the 10 nm thick sample increased with the highest rate, from 21.7 to 25.0 ^{o}C, while the other samples also gave similar temperature increments but at a lower rate [see Fig. 7(a)]. This result can be explained by considering the fact that a thicker thin film is more reflective. Hence a larger portion of the energy is reflected backwards, thus resulting in less heat conversion through plasmon absorption. Meanwhile, the temperature variation is extremely sensitive to the switch of laser beam [see Fig. 7(b)]. Such results further confirm the existence of local optical heating, which yields convective flow and thermophoresis simultaneously.

In summary, the trapping phenomenon has several unique characteristics namely: (i) Initially, an increase in the incident laser power resulted in larger number of PS being trapped. The trend then reaches a peak, and further increase of laser power actually caused the size of the cluster to shrink. Eventually, this would cause the trap to disappear. In fact further increase of laser power resulted in the formation of a gas bubble on the Au film. All samples of different Au film thicknesses exhibited similar behaviour, except that they required different thresholds for maximum cluster size and bubble generation. (ii) For the case of 10 nm Au thin film, the rate of temperature increase as inferred from fluorescence data was the highest among all samples (see Fig. 7). However, as revealed from Fig. 6, within experimental errors all samples exerted similar drag force on the colloidal PS for a given incident laser power. Furthermore, 70 nm Au thin film offered the largest number of trapped PS for a given laser power, while 10 nm Au gave the smallest. (iii) Fig. 1a shows that within the range of 10 to 70 nm, absorption coefficient increases with Au film thickness. This means that for the 10 nm case, relatively less heat is deposited to the illuminated region.

Based on the above observations, we conclude that convective force is primarily originated from flow of solvent surrounding the hot zone induced through plasmonic absorption in the Au film. Our experiments suggest that drag force is relatively insensitive to the Au film thickness. However, since the flow velocity varies dramatically with distance from the surface because of the presence of a boundary layer, it is likely that the drag force as deduced from monitoring the movement of PS is merely a measure of long-range flow distribution well away from the hot zone. Furthermore, temperature mapping through

fluorescence measurement has been viewed as an underestimation of the actual surface temperature, and this technique is quite reliable for providing relative information between samples and monitoring changes in temperature.[28, 42, 43] This explains why we were able to generate a bubble on the film when the laser power was sufficiently high, as the actual surface temperature must be close to boiling point of water. For the current experiments, the higher surface temperature recorded in the 10 nm case can be explained by considering the relatively smaller volume of gold involved in the heat generation process. As the Au film is sandwiched between water and glass which are of lower thermal conductivities, the heat energy deposited in the film through plasmonic absorption will lead to larger temperature rise if a smaller volume of gold is being illuminated. On the other hand, for the 70 nm case, while the rise in surface temperature may be relatively less significant because of larger volume of gold involved, the film has larger absorption coefficient and there will be higher percentage of energy deposited in the hot zone for a given laser power level. Consequently, the size of the hot zone becomes larger, which in turn results in a larger trap size. Nonetheless, the intuitive analysis presented here may not necessarily be a comprehensive model as there must be an intricate dynamic balance between heat flow pathways through diffusion, which is currently being taken as the origin for thermophoretic forces, and convection.

In addition to the above, our experiments also show that trapping can be achieved with laser wavelengths other than 785 nm. Figure 8 presents the frame images of trapped PS recorded from samples with nominally 10 to 70 nm continuous gold films and excitation lasers at λ=785 nm with focus size of 1.0 μm [Fig. 8(a)], at λ=532 nm with focus

size of 3.8 μm [Fig. 8(b)], and at λ=473 nm with focus size of 3.2 μm [Fig. 8(c)], respectively, from the images one can see that the diameter of trapped colloidal assembly is always larger than that of the laser focus spot. This result further confirms that trapping of PS is dominated by thermal effects. In addition, all of the three wavelengths have been found to be effective in producing the trapping phenomenon. We attribute this to the fact that the continuous gold thin films have broadband absorption spectra [see Fig. 1(a)], which ensure that plasmon absorption heating is always present. It should also be mentioned that in the case of Fig. 8(a) we used a 60X oil lens and 0.5 μm PS, while in the cases of Fig. 8(b) and 8(c) we used 40× lens and 1.5 μm PS. We introduced the changes in order to achieve better trapping performance in terms of trap capacity and the compactness of the assembly. Actually, trapping of 0.5 μm PS can also be achieved with 532 nm and 473 nm laser beams and a large NA objective, but with a reduction in trap capacity. We attribute this to the fact that the contributions from thermophoresis and convection may vary at different degree with the size of the target particles according to excitation conditions.

The influence of salt concentration on the trapping behaviour has also been studied. Figure 9 shows the number of trapped PS particles as a function of salt concentration for the 30 nm and 50 nm cases respectively. First, we can see that the number of PS being trapped always reaches its maximum when the solution has zero salt concentration (deionized water). Second, as the salt concentration gradually increases, the number of trapped PS decreases fast until it reaches zero at 10^{-4} mol, which means that the trapping effect has been quenched at this concentration level. This also happens for the 10 nm and

70 nm cases. We attribute this to the change of thermophoresis. Even though thermophoresis has been regarded as peculiarly sensitive in many reported systems and a comprehensive understanding of this environment-specific system requires further investigation, a number of experimental results have confirmed that thermophoretic forces can be significantly modified in terms of magnitude and even direction by adding salt into the colloidal suspension.[21, 22, 25, 44, 45] In the present case, with the ionic property of the solution gradually enhanced, the thermophoretic force is reduced until it cannot overcome the axial upward convective drag force so that the trapping phenomenon disappears, which coincides with those trapping schemes by using thermophoresis and convection.[45, 46]

Conclusions

In summary, we have demonstrated the trapping and assembling of colloidal crystal on continuous gold thin films based on thermophoresis and thermal convection induced by plasmonic heating. In particular, the thermophoretic force pushing the PS from cold to hot region is larger than the axial convective drag force, therefore stabilizing the trap for a long period of time. Furthermore, the lateral convection also plays a positive role by dragging more PS into the hot region from a long distance and thus supplying and accelerating the trap considerably. The influence of salt concentration on the trapping behaviour has also been investigated. It is found that salt concentration of 10^{-4} mol or higher will significantly weaken the strength of the thermophoretic force, which cannot counter balance the upward axial convective drag force and the trapping effect finally

disappears. Since the threshold power is as low as several microwatts per square micron and the trapping effect is very effective and stable, we anticipate that the reported technique may inspire many relevant applications in biophysics, life science, and lab-on-a-chip devices.[43]

Acknowledgement

The authors acknowledge the financial support from a Collaborative Research Fund (CUHK1/CRF/12G) and an Area of Excellence Grant (AoE/P-02/12) provided by the Research Grants Council (RGC) of Hong Kong SAR of China. A research studentship (JJ Chen) from The Chinese University of Hong Kong is gratefully acknowledged.

References

1. A. Ashkin, J. M. Dziedzic, J. E. Bjorkholm and S. Chu, *Opt. Lett.*, 1986, **11**, 288-290.
2. D. G. Grier, *Nature*, 2003, **424**, 810-816.
3. T. T. Perkins, *Laser Photonics Rev*, 2009, **3**, 203-220.
4. K. C. Neuman and S. M. Block, *Rev. Sci. Instrum.*, 2004, **75**, 2787-2809.
5. A. N. Grigorenko, N. W. Roberts, M. R. Dickinson and Y. Zhang, *Nat. Photon.*, 2008, **2**, 365-370.
6. M. Righini, G. Volpe, C. Girard, D. Petrov and R. Quidant, *Phys. Rev. Lett.*, 2008, **100**, 186804.
7. M. L. Juan, M. Righini and R. Quidant, *Nat. Photon.*, 2011, **5**, 349-356.
8. J. Berthelot, S. S. Acimovic, M. L. Juan, M. P. Kreuzer, J. Renger and R. Quidant, *Nat. Nanotech.*, 2014, **9**, 295-299.
9. W. H. Zhang, L. N. Huang, C. Santschi and O. J. F. Martin, *Nano Lett.*, 2010, **10**, 1006-1011.
10. B. J. Roxworthy, K. D. Ko, A. Kumar, K. H. Fung, E. K. C. Chow, G. L. Liu, N. X. Fang and K. C. Toussaint, *Nano Lett.*, 2012, **12**, 796-801.
11. T. Shoji, M. Shibata, N. Kitamura, F. Nagasawa, M. Takase, K. Murakoshi, A. Nobuhiro, Y. Mizumoto, H. Ishihara and Y. Tsuboi, *J. Phys. Chem. C.*, 2013, **117**, 2500-2506.
12. K. Y. Chen, A. T. Lee, C. C. Hung, J. S. Huang and Y. T. Yang, *Nano Lett.*, 2013, **13**, 4118-4122.
13. Z. W. Kang, H. X. Zhang, H. F. Lu, J. B. Xu, H. C. Ong, P. Shum and H. P. Ho, *Opt. Lett.*, 2012, **37**, 1748-1750.
14. L. Huang, S. J. Maerkl and O. J. F. Martin, *Opt. Express*, 2009, **17**, 6018-6024.

15. Z. W. Kang, H. F. Lu, J. J. Chen, K. Chen, F. Xu and H. P. Ho, *Opt. Express*, 2014, **22**, 19567-19572.
16. J. J. Chen, Z. W. Kang, H. F. Lu, H. X. Zhang, W. C. H. Choy, N. K. Chen and H. P. Ho, *Vacuum*, 2015, **118**, 171-176.
17. K. Wang, E. Schonbrun, P. Steinvurzel and K. B. Crozier, *Nat. Commun.*, 2011, **2**, 469.
18. J. S. Donner, G. Baffou, D. McCloskey and R. Quidant, *Acs Nano*, 2011, **5**, 5457-5462.
19. B. J. Roxworthy, A. M. Bhuiya, S. P. Vanka and K. C. Toussaint, *Nat. Commun.*, 2014, **5**, 3173.
20. J. C. Ndukaife, A. Mishra, U. Guler, A. G. A. Nnanna, S. T. Wereley and A. Boltasseva, *Acs Nano*, 2014, **8**, 9035-9043.
21. R. Piazza and A. Parola, *J Phys-Condens Mat*, 2008, **20**, 153102.
22. R. Piazza, *Soft Matter*, 2008, **4**, 1740-1744.
23. M. Braibanti, D. Vigolo and R. Piazza, *Phys. Rev. Lett.*, 2008, **100**, 108303.
24. S. Iacopini and R. Piazza, *Europhys Lett*, 2003, **63**, 247-253.
25. S. A. Putnam and D. G. Cahill, *Langmuir*, 2005, **21**, 5317-5323.
26. E. E. Michaelides, *Int J Heat Mass Tran*, 2015, **81**, 179-187.
27. L. Helden, R. Eichhorn and C. Bechinger, *Soft Matter*, 2015, **11**, 2379-2386.
28. Z. W. Kang, J. J. Chen, S. Y. Wu, K. Chen, S. K. Kong, K. T. Yong and H. P. Ho, *Sci. Rep.*, 2015, **5**, 9978.
29. S. Ducourtieux, V. A. Podolskiy, S. Gresillon, S. Buil, B. Berini, P. Gadenne, A. C. Boccara, J. C. Rivoal, W. D. Bragg, K. Banerjee, V. P. Safonov, V. P. Drachev, Z. C. Ying, A. K. Sarychev and V. M. Shalaev, *Phys. Rev. B*, 2001, **64**, 165403.
30. G. Q. Liu, Z. Q. Liu, Y. H. Chen, Z. J. Cai, Y. Hu, X.N. Zhang, and K. Huang, Sci. Adv. Mater., 2014, **6**, 1099-1105.
31. Z. Liu, M. Yu, S. Huang, X. Liu, Y Wang, M. Liu, P. Pana and G. Liu, J. Mater. Chem. C, 2015,**3**, 4222-4226.
32. B. Ding, C. Hrelescu, N. Arnold, G.Isic, and T. A. Klar, Nano Lett., 2013, **13**, 378-386.
33. L. Shi, X. Liu, H. Yin, and J. Zi, Phys. Lett. A, 2010, 374, 1059-1062.
34. B. Ding, M. E. Pemble, A. V. Korovin, U. Peschel, and S. G. Romanov, Phys. Rev. B, 2010 82, 035119.
35. Z. W. Kang, H. X. Zhang, H. F. Lu and H. P. Ho, *Plasmonics*, 2013, **8**, 289-294.
36. X. G. Ma, P. Y. Lai and P. G. Tong, *Soft Matter*, 2013, **9**, 8826-8836.
37. C. Min, Z. Shen, J. Shen, Y. Zhang, H. Fang, G. Yuan, L. Du, S. Zhu, T. Lei, and X. Yuan, Nat. Commun., 2013, **4,** 2891.
38. L. Korson, Drosthan.W and F. J. Millero, *J. Phys. Chem.*, 1969, **73**, 34-39.
39. B. J. Roxworthy and K. C. Toussaint, *Opt. Express*, 2012, **20**, 9591-9603.
40. F. Lemoine, Y. Antoine, M. Wolff and M. Lebouche, *Exp. Fluids*, 1999, **26**, 315-323.
41. C. H. Fang, L. Shao, Y. H. Zhao, J. F. Wang and H. K. Wu, *Adv. Mater.*, 2012, **24**, 94-98.
42. J. J. Chen, Z. W. Kang, S. K. Kong and H. P. Ho, *Opt. Lett.*, 2015, **40**, 3926-3929.
43. J. J. Chen, Z. W. Kang, G. H. Wang, J. F. C. Loo, S. K. Kong and H. P. Ho, *Lab Chip*, 2015, **15**, 2504-2512.
44. D. Vigolo, R. Rusconi, H. A. Stone and R. Piazza, *Soft Matter*, 2010, **6**, 3489-3493.
45. S. Duhr and D. Braun, *Appl. Phys. Lett.*, 2005, **86**, 131921.
46. D. Braun and A. Libchaber, *Phys. Rev. Lett.*, 2002, **89**, 188103.

Figure Captions:

Figure 1. (a) Right: Optical images of continuous gold thin film samples with thickness of 10, 30, 50, and 70 nm, respectively. Left: Their corresponding extinction spectra. (b-e) Atomic force microscope (AFM) images of all samples, with RMS (root mean square) of roughness shown at the top.

Figure 2. Schematic illustration of the experiment. Thermal convection pushes the aqueous medium laterally into the hot zone and then axially out of the zone. Thermophoresis drives the PS from cold to hot region with a force magnitude larger than that of the axial convective drag force.

Figure 3. Successive image frames showing the trapping of PS in the 30 nm (a) and 50 nm (b) samples, both at P3 (9.2 mW). Laser beam switched on at t=0 s and switched off immediately before the last frame.

Figure 4. (a-d) Statistical analysis of the trapped PS at different laser power levels as a function of time for 10, 30, 50, and 70 nm samples respectively. (e) Statistical analysis of the trapped particles as a function of time for 0.5 μm and 1.5 μm PS diameter using laser power P2. Solid lines are exponential fitting to experiment data.

Figure 5. Image showing trapping on 50 nm sample with the use of small NA (=0.6) objective and laser power 3.7 mW (P2), PS diameter at 1.5 μm and concentration of

4×10^7 particles/mL. Objective lens: 40×.

Figure 6. Time-averaged velocity of PS and convective drag force as a function of incident laser power for all samples. Error bars denote experimental standard deviations.

Figure 7. (a) Temperature variation as a function of laser power. Error bars denote experimental standard deviations. (b) Temporal response of temperature in 10 nm sample as a function of time. Laser power: 41.6 mW (P5).

Figure 8. Frame images of trapped PS assembly on all samples. Laser focal spot size (diameter): 1 μm at λ=785 nm (a), 3.8 μm at λ=532 nm (b), and 3.2 μm at λ=473 nm (c), respectively. For case (a), PS diameter: 0.5 μm, objective lens: 60× with NA=1.49 (oil immersion). For cases (b) and (c), PS diameter: 1.5 μm, objective lens: 40× lens with NA=0.6.

Figure 9. Number of trapped PS as a function of salt concentration for 30 nm and 50 nm samples respectively. Laser power: P3 (9.2 mW). Error bars denote experimental standard deviations.

Figure 1

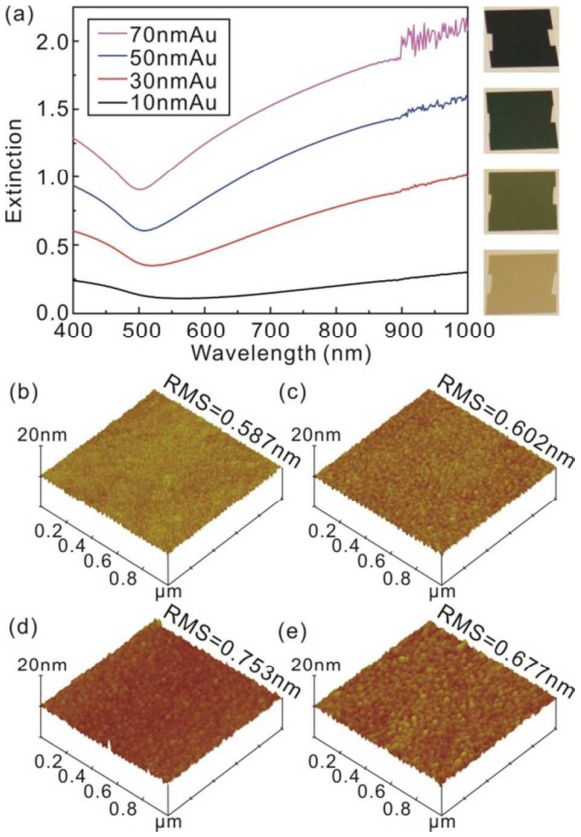

Figure 2

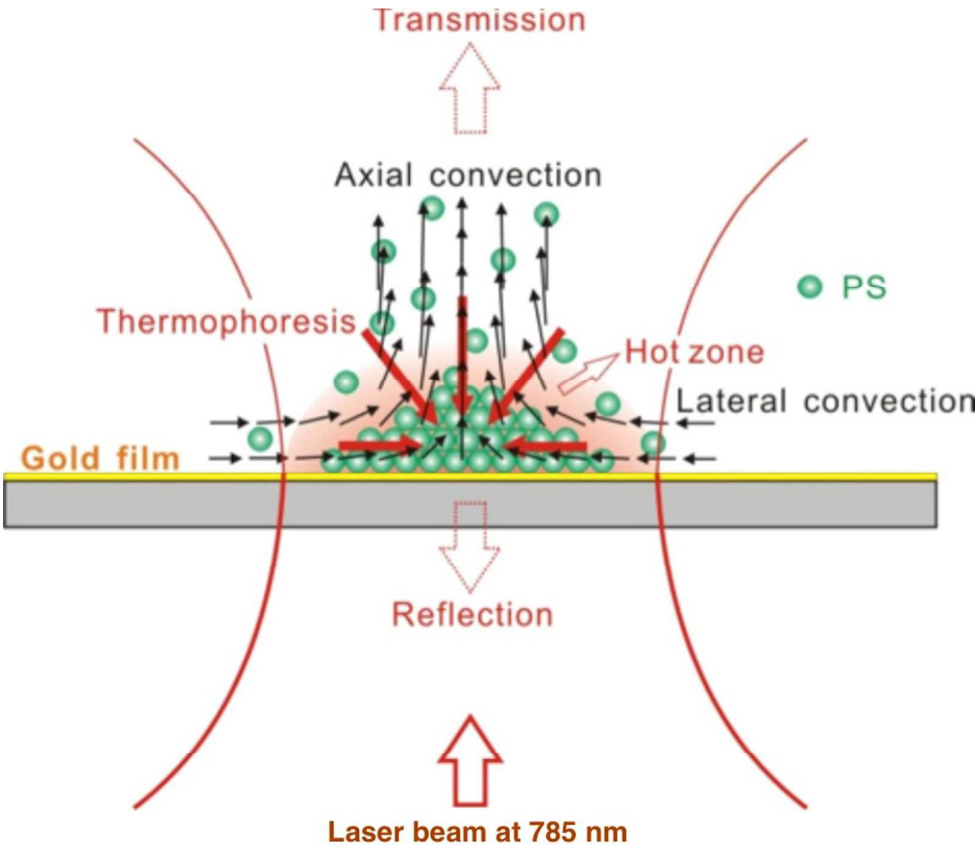

Figure 3

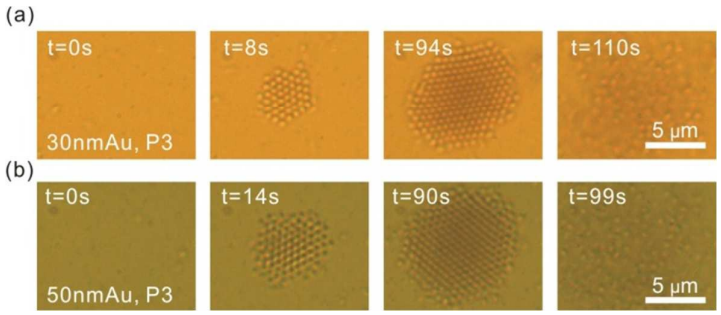

Figure 4

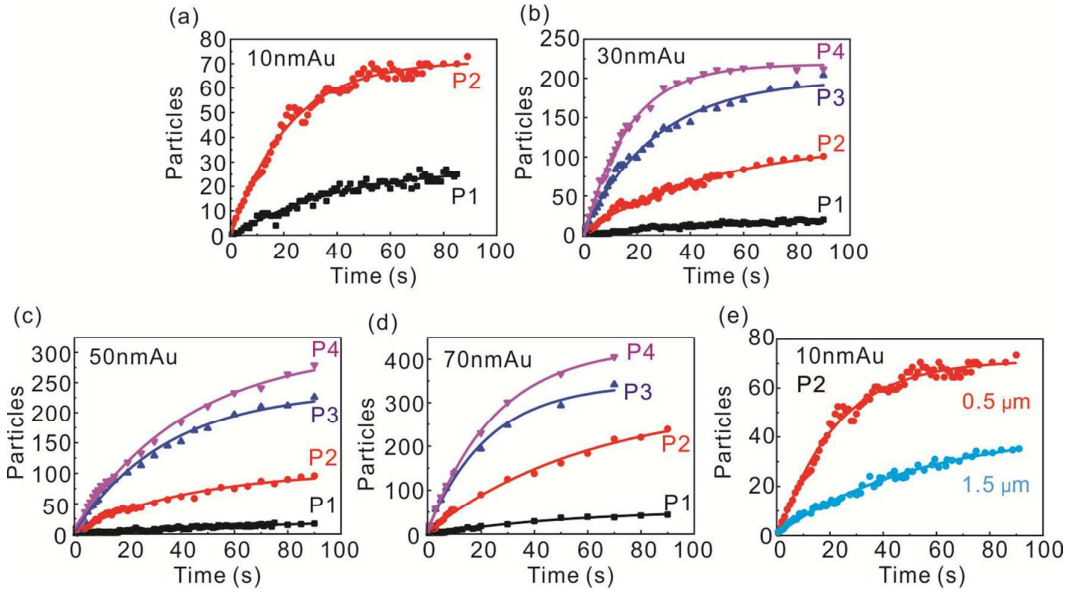

Figure 5

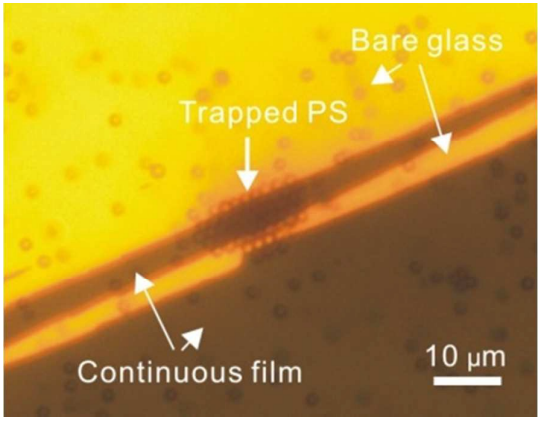

Figure 6

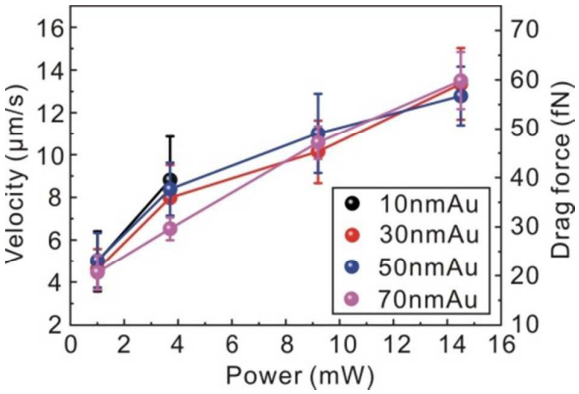

Figure 7

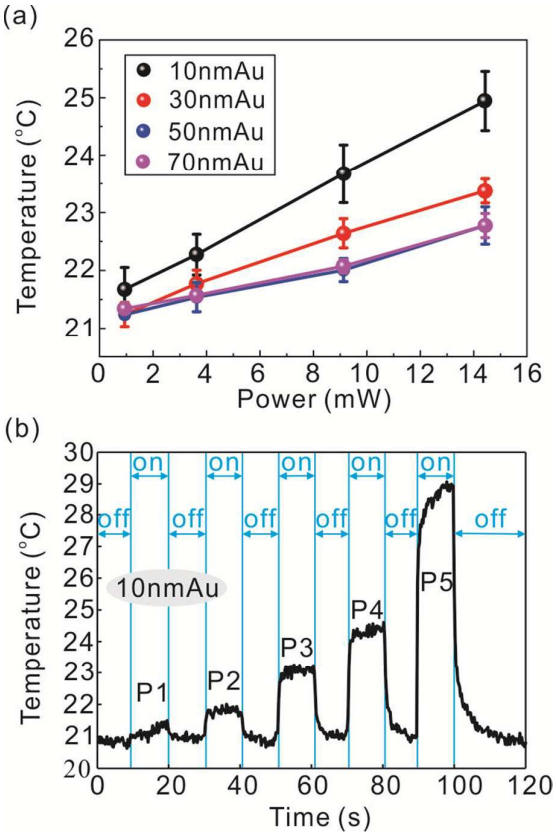

Figure 8

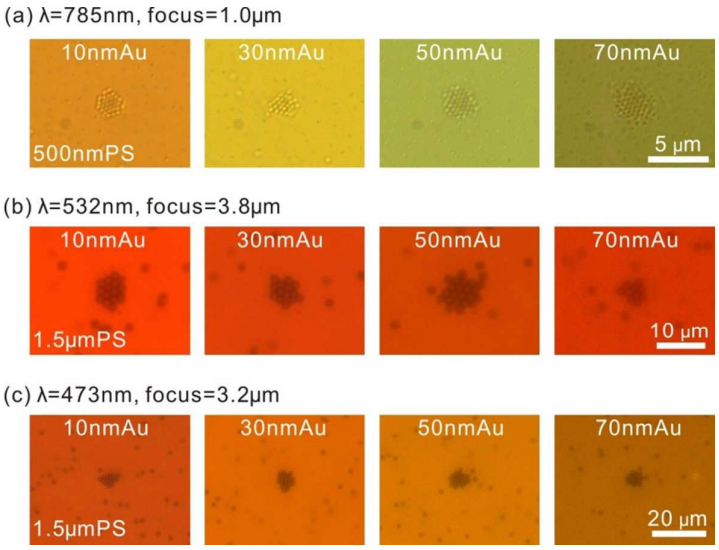

Figure 9

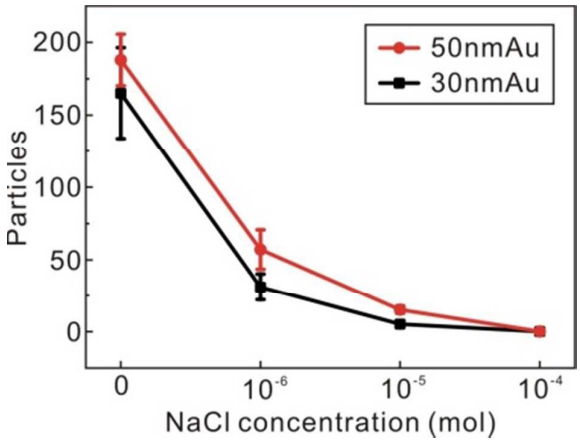

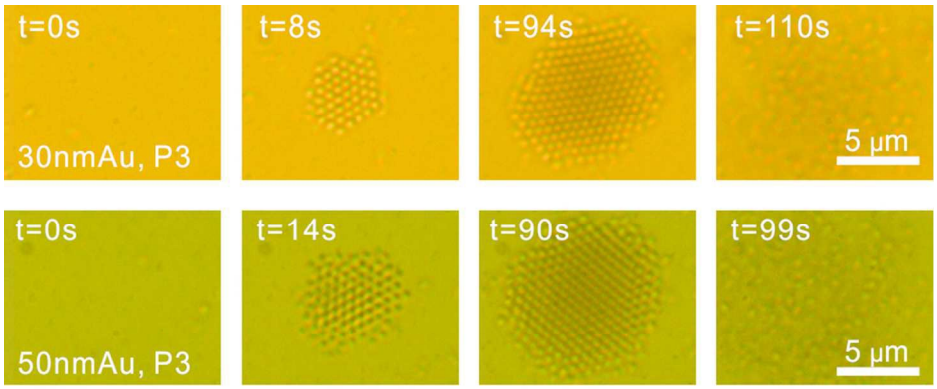

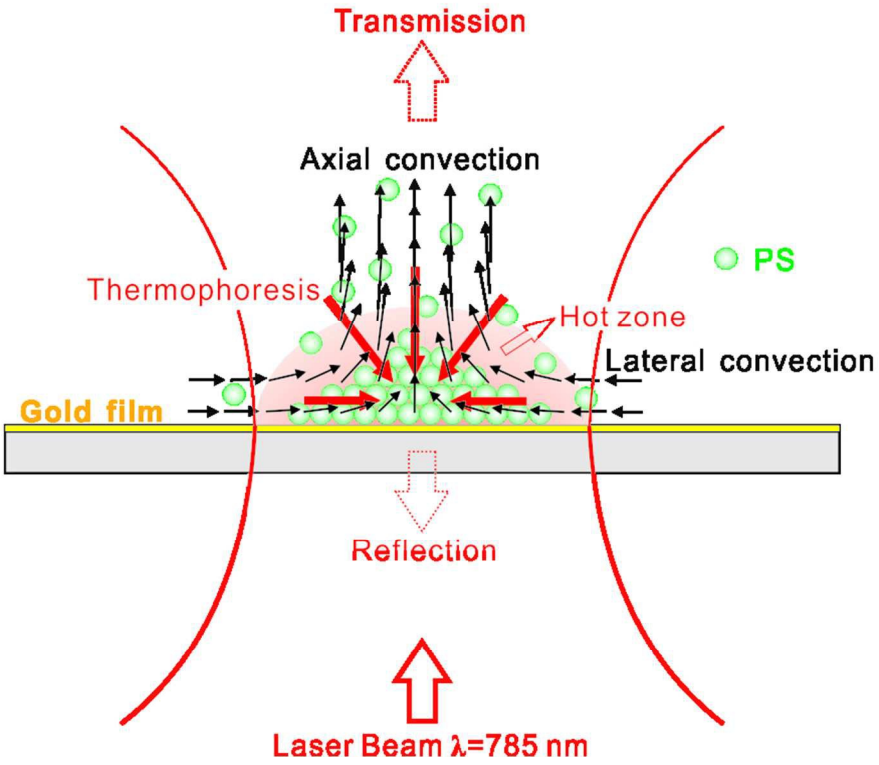

78x101mm (300 x 300 DPI)